doi:10.1111/j.1558-5646.2007.00278.x

EVOLUTION OF THE GENOMIC RATE OF RECOMBINATION IN MAMMALS

Beth L. Dumont[1] and Bret A. Payseur[1,2]

[1] *University of Wisconsin-Madison, Laboratory of Genetics, 425-GHenry Mall, Madison, Wisconsin 53706*

[2] *E-mail: payseur@wisc.edu*

Received August 13, 2007
Accepted October 2, 2007

Rates of recombination vary considerably between species. Despite the significance of this observation for evolutionary biology and genetics, the evolutionary mechanisms that contribute to these interspecific differences are unclear. On fine physical scales, recombination rates appear to evolve rapidly between closely related species, but the mode and tempo of recombination rate evolution on the broader scale is poorly understood. Here, we use phylogenetic comparative methods to begin to characterize the evolutionary processes underlying average genomic recombination rates in mammals. We document a strong phylogenetic effect in recombination rates, indicating that more closely related species tend to have more similar average rates of recombination. We demonstrate that this phylogenetic signal is not an artifact of errors in recombination rate estimation and show that it is robust to uncertainty in the mammalian phylogeny. Neutral evolutionary models present good fits to the data and we find no evidence for heterogeneity in the rate of evolution in recombination across the mammalian tree. These results suggest that observed interspecific variation in average genomic rates of recombination is largely attributable to the steady accumulation of neutral mutations over evolutionary time. Although single recombination hotspots may live and die on short evolutionary time scales, the strong phylogenetic signal in genomic recombination rates indicates that the pace of evolution on this scale may be considerably slower.

KEY WORDS: **Genetic maps, mammalian genomics, phylogenetic comparative methods, recombination.**

The rate of recombination varies substantially among sexual eukaryotes. At one end of this spectrum, the yeast *Saccharomyces cerevisiae* recombines at an average rate of 340 cM/Mb, and toward the other extreme, the human genome undergoes an average of just over 0.01 crossovers per megabase of DNA sequence (Cherry et al. 1997; Broman et al. 1998; Kong et al. 2002). Even among closely related mammals there is striking interspecific variation. On average, the human genome experiences twice as much recombination per meiosis as the mouse genome (Dietrich et al. 1996; Broman et al. 1998; Kong et al. 2002; Shifman et al. 2006), and over five times that of the domestic opossum (Samollow et al. 2004).

These recombination rate differences bear on several fundamental issues in evolutionary biology. First, the rate of recombination shapes the fates of selected and neutral mutations in populations (Fisher 1930; Muller 1932; Hill and Robertson 1966; Felsenstein 1974). By decoupling beneficial alleles from linked deleterious variation, recombination accelerates the rate of fixation of high fitness genotypes (Crow and Kimura 1965; Maynard Smith 1971). At the same time, recombination also increases the effectiveness of selection against deleterious mutations (Muller 1964; Kondrashov 1988; Haddrill et al. 2007). These considerations have made the rate of recombination a key parameter in models of the evolution of sexual reproduction (Michod and Levin 1988). Furthermore, the reduction of linked neutral diversity that accompanies the fixation of beneficial mutations (genetic hitchhiking) or the removal of deleterious mutations (background selection) depends on the recombination rate (Maynard Smith and Haigh 1974; Charlesworth et al. 1993).

Recombination is also a fundamental determinant of patterns of haplotype diversity across genomes. On average, species with higher recombination rates (but similar effective population sizes)

are expected to exhibit less linkage disequilibrium. Therefore, the ability to infer evolutionary history using patterns of linkage disequilibrium (Haddrill et al. 2005; Voight et al. 2006), including the identification of genetic variants that control phenotypic variation through association mapping (The International HapMap Consortium 2005), will differ between species.

Despite the central significance of recombination rate to evolution, little is known about how differences between species arise (but see True et al. 1996 for a detailed discussion). Rates of recombination are readily modified by artificially imposed selection pressures in laboratory populations of *Drosophila* (Detlefson and Roberts 1921; Parsons 1958; Mukherjee 1961; Chinnici 1971; Kidwell 1972; Brooks and Marks 1986), and domesticated plant species tend to have altered rates of recombination as compared with their wild progenitors (Ross-Ibarra 2004). These empirical observations suggest that levels of divergence in recombination rates could reflect the action of unique selective regimes in different species, but the importance of selection on rates of recombination in nature remains largely unknown. Theoretical studies indicate that selection can favor altered rates of recombination in novel (reviewed in Burt 2000), marginal (Lenormand and Otto 2000), or rapidly fluctuating environments (Charlesworth 1976; Barton 1995; Peters and Lively 1999; Lenormand and Otto 2000), but empirical support for these findings is wanting. Alternatively, variation in recombination rates between species could mostly arise through the accumulation of neutral mutations over time.

Recently, comparative genomic approaches have offered clues into the evolutionary dynamics of recombination. Rates measured across orthologous 5 Mb regions in mouse, rat, and human are only weakly positively correlated between species, indicating that the shared evolutionary history of a genomic region may be a poor predictor of recombination rate (Jensen-Seaman et al. 2004). Similarly, comparisons of fine-scale recombination rates inferred from patterns of polymorphism in human and chimpanzee populations reveal weak to no correlation between recombination rate profiles over homologous intervals (Ptak et al. 2004, 2005; Winckler et al. 2005). PCR-based methods for measuring fine-scale recombination rates from large numbers of sperm have also exposed differences in recombination rates among laboratory strains of mice (Shiroishi et al. 1995; Yauk et al. 2003; Baudat and de Massy 2007), and even highlighted rate differences between individuals within single human populations (Jeffreys et al. 1998; Jeffreys and Neumann 2002; Neumann and Jeffreys 2006). Together, these observations suggest that local recombination rates can evolve on short evolutionary time scales.

Whether this pattern of rapid evolution extends to broader scale recombination rates is unknown. In mammals, broad-scale recombination rates are constrained by the meiotic mechanisms that regulate the disjunction of homologous chromosomes (reviewed in Coop and Przeworski 2007). A minimum of one chiasma per chromosome arm must form to maintain homologue pairing during meiosis in the face of the polarizing forces that emanate from the meiotic spindle (Mather 1938; Jones 1984). Failure to meet this requirement frequently results in cell death or aneuploid gametes, and mutations leading to systemic errors in the distribution and number of chiasma at meiosis are frequent causes of infertility and subfertility in a large number of species (Micic et al. 1982; Zetka and Rose 1995; Koehler et al. 1996; Hassold and Hunt 2001; Shah et al. 2003). The tight link between genomic recombination rates and organismal fitness suggests that the rate of evolution at this scale could be considerably slower.

In this article, we apply phylogenetic comparative methods and quantitative evolutionary models to address two key issues in the evolution of average genomic rates of recombination in mammals. First, we ask whether rates of recombination measured at the level of entire genomes display a phylogenetic signal. Second, we test the hypothesis that neutral evolution gave rise to the observed distribution of genomic recombination rates in mammals. Our study provides the first phylogenetic analysis of recombination rate evolution in mammals and provides insights into the evolutionary origins of species differences in recombination rates.

Materials and Methods

GENETIC MAPS

Thirteen mammalian species featuring sex-averaged genetic maps were identified from the primary literature (Table 1). Five mammalian orders within the infraclass Eutheria are represented—primates (human, hamadryas baboon, rhesus macaque), rodents (mouse, rat), carnivores (cat, dog), perissodactyls (horse), and artiodactyls (pig, cow, sheep)—along with two metatherian species (gray short-tailed opossum and tammar wallaby).

ASSESSING GENETIC MAP COVERAGE

Method 4 of Chakravarti et al. (1991) was applied to correct for variation in marker density among mammalian genetic maps and we account for undetected crossover events occurring distal to terminal markers using the method of Hall and Willis (2005). The average percentage of the genome that lies within d cM of a marker was calculated under the assumption of random marker distribution. This percentage is given by

$$(1 - e^{-2dn/L}) \times 100\%$$

where n is the number of markers on the map, and L is the uncorrected estimate of total genetic map length in centiMorgans (Hall and Willis 2005).

PHYSICAL GENOME SIZE ESTIMATES

Estimates of total physical genome size in megabase were drawn from the completed genome assemblies of human (Lander et al.

Table 1. Mammalian genetic maps.

Species	Order	Genetic map length (cM)[1]	Number of markers	Average intermarker interval (cM)	Average number of informative meioses[2]	Reference
Human	Primates	3615	5136	0.704	880	(Kong et al. 2002)
Baboon	Primates	2013	352	5.719	865	(Rogers et al. 2000)
Macaque	Primates	2275	326	6.979	NA[5]	(Rogers et al. 2006)
Mouse	Rodentia	1361	6336	0.215	92	(Dietrich et al. 1996)
Rat	Rodentia	1542	3824	0.403	41.4	(Steen et al. 1999)
Horse	Perissodactyla	2770	742	3.733	71.8	(Swinburne et al. 2006)
Cat	Carnivora	3300[3]	253	13.043	82	(Menotti-Raymond et al. 1999)
Dog	Carnivora	3884[4]	2773	1.401	297	(Neff et al. 2006)
Pig	Artiodactyla	2286	1042	2.194	78	(Rohrer et al. 1996)
Sheep	Artiodactyla	3588	1015	3.535	128	(Maddox et al. 2001)
Cow	Artiodactyla	3160	3960	0.798	203	(Ihara et al. 2004)
Wallaby	Diprotodontia	829	64	12.953	353	(Zenger et al. 2002)
Opossum	Didelphimorphia	644	83	7.759	162	(Samollow et al. 2004)
CFTR	–	H_P^2=0.810 P=0.041	H_P^2=0.0003 P=0.256	–	H_P^2=1.00 P=0.002	–
Mitochondria	–	H_P^2=1.00 P=0.004	H_P^2=0.0003 P=0.235	–	H_P^2=1.00 P=0.022	–

[1] Sex-averaged.
[2] When not explicitly given in the reference, we use the total number of meioses multiplied by the average heterozygosity across markers as an estimate.
[3] Actual total genetic map length is 2040 cM, but adjusting this total for unrepresented dot chromosomes and marker poor chromosomes yields an estimated sex-average genetic map length of 3300 cM.
[4] Autosomal map length from listed reference plus X chromosome map length taken from (Neff et al. 1999).
[5] Due to missing data in macaque, the H_P^2 of the average number of informative meioses was calculated using an ML tree constructed without macaque.

2001; Venter et al. 2001), dog (Lindblad-Toh et al. 2005), macaque (Gibbs et al. 2007), mouse (Waterston et al. 2002), rat (Gibbs et al. 2004), and opossum (Mikkelsen et al. 2007). The genome sizes of cow and horse were derived from predictions based on draft genome assemblies (http://www.hgsc.bcm.tmc.edu/projects/bovine/; http://www.broad.mit.edu/mammals/horse/), and the pig estimate of 3000 Mb was taken from the Porcine Genome Sequencing White Paper (Rohrer et al. 2002). The projected length of the wallaby genome is 3.6–3.8 Gb (Hayman and Martin 1974; Marshall Graves et al. 2004) and we used an intermediate value of 3.7 Gb in our analyses. Estimates of genome size based on DNA weight indicate that the baboon genome is comparable in size to that of other sequenced primates, and that sheep and cow have similarly sized genomes (Gregory 2007). Therefore, we approximated the genome size of baboon with that of macaque and assumed that cow and sheep have equally sized genomes.

BODY SIZE ESTIMATES

The evolution of body weight in mammals has been heavily studied and is well-characterized (Smith et al. 2004). We collected sex-average adult body weights (in grams) for each species from the literature (Nowak 1999a, b) to provide a comparison to the evolutionary patterns we found in recombination rates. Weight measurements were natural log transformed to improve fit to normality.

MAMMALIAN PHYLOGENIES

The availability of large molecular sequence datasets coupled with advances in phylogenetic inference has spurred recent progress in the understanding of the evolutionary relationships among mammals (reviewed in Springer et al. 2004). Despite the large number of mammalian phylogenies that have been previously published, none include all 13 species with dense genetic maps. For this reason, we generated our own mammalian phylogenies using the two datasets that feature sequence data for the complete group of 13 species—CFTR coding sequence and 13 mitochondrial protein-coding gene sequences.

A multi-species sequence alignment including each of the 13 species with genetic maps and an outgroup (platypus) was produced from approximately 4.5 kb of coding sequence from the CFTR gene (see online Supplementary Table S1). Sequences were aligned using CLUSTAL-W (Thompson et al. 1994) and the resulting alignment was verified by eye. We used the maximum-likelihood (ML) methods implemented in the program phyml to

generate phylogenies under 35 unique models of nucleotide substitution (Guindon and Gascuel 2003) (see online Supplementary Table S2). A general time-reversible (GTR) model of molecular evolution with a gamma distribution of rates across four classes (rate parameter estimate obtained by ML) and ML estimates of base frequencies yielded the best tree, as assessed by both Akaike and Bayes' information criteria (AIC and BIC, respectively; Fig. 2A). Nodal support was assessed using 1000 bootstrap replicates. Individual bootstrap replicates were retained for further analyses (see below).

We generated a second mammalian phylogeny using mitochondrial sequence data from each of the 13 species and platypus. Coding sequences from 13 mitochondrial protein-coding genes were obtained from the mammalian mitochondrial genomics database (http://www.mammibase.lncc.br/home.php), manually concatenated, and aligned using CLUSTAL-W (Thompson et al. 1994). Again, we constructed phylogenies under 35 unique models of molecular evolution using phyml and discriminated among the resultant trees using the AIC and BIC (see online Supplementary Table S3). A GTR model with a gamma distribution of rates across four classes (rate parameter estimated using ML), an estimated proportion of invariant sites, and ML estimates of nucleotide frequencies was optimal by these selection criteria (Fig. 2B). Due to computational constraints imposed by the size of this dataset, node support was assessed using just 100 bootstrap replicates. Individual replicates were again retained for additional analyses.

The outgroup species platypus was included in the process of phylogeny construction to root the basal relationship between Metatheria and Eutheria. We pruned the lineage leading to platypus following the construction of both ML trees and derived the corresponding phylogenetic variance–covariance matrices using the vcv.phylo function in the ape contributed package to the R environment for statistical computing (Paradis et al. 2004; R Development Core Team 2006).

MIXED MODEL COMPARATIVE METHOD

The mixed model approach of Lynch (1991) uses the variance–covariance phylogenetic relations among species and a Brownian motion model of quantitative character evolution to partition each realized phenotypic value, z, into three components

$$z_i = u + a_i + e_i$$

where u is the phenotypic component shared by all members of the phylogeny, a_i is the heritable additive effect of the character in the i^{th} taxon, and e_i is a residual error term that captures variation due to measurement error, phylogenetic uncertainty, phenotypic plasticity, rapid evolution along terminal branches, and fluctuating selection. ML estimates of $\hat{u}$, $\hat{a}_i$, and $\hat{e}_i$ were obtained using the EM algorithm with convergence established when successive iterations yielded parameter estimates that differed by less than 1×10^{-4}.

The variances associated with the heritable additive and error terms, σ_a^2 and σ_e^2, are combined to provide an estimate of phylogenetic heritability

$$H_p^2 = \frac{\sigma_a^2}{\sigma_a^2 + \sigma_e^2}.$$

In our analyses, H_P^2 is the proportion of variation in recombination rate that is attributable to the underlying phylogeny. It quantifies the degree to which knowledge of the recombination rate in one species provides predictive information about the rate in a second species.

Permutation tests were used to calculate P-values for H_P^2 estimates. Recombination rates were randomly shuffled with respect to species designations at the tips of the tree whereas the underlying topology and branch lengths were kept constant. We then recomputed the phylogenetic heritability on the permuted dataset and determined the quantile position of our observed value along the distribution of permuted values. A total of 10,000 permutations were used to assess significance in all cases, with the exception of total genetic map length, physical genome size, marker number and the average number of informative meioses. Computational constraints reduced the number of permutations to 1000 for these quantities. All analyses were performed in the R environment for statistical computing using base package functions and function calls within the ape contributed package (Paradis et al. 2004; R Development Core Team 2006).

ASSESSING LINEAGE-SPECIFIC EVOLUTIONARY PATTERNS

We constructed ML trees using subsets of the CFTR and mitochondrial sequence alignments to evaluate the contribution of specific lineages to the evolutionary patterns we find. In particular, we built trees that exclude the two metatherian taxa and trees that exclude the two rodent species, as these lineages harbor especially low rates of recombination relative to other mammalian species. We reran CLUSTAL-W on each partial sequence dataset to generate the corresponding optimal alignment. As before, we considered 35 models of molecular evolution using phyml to identify the evolutionary model providing the best fit to each partial sequence dataset. For both the CFTR and mitochondrial trees excluding the two metatherian species, a GTR model with a gamma distribution of rates across four classes and a proportion of invariant sites is preferred, as assessed by the AIC and BIC. The same model yielded the lowest AIC and BIC for the mitochondrial tree excluding the two rodents, but a GTR model with a gamma distribution of rates across four classes provided the best fit to the CFTR sequence dataset that excludes mouse and rat.

MEASURING THE EFFECTS OF PHYLOGENETIC UNCERTAINTY

Several additional phylogenies were considered to assess the robustness of documented evolutionary trends to uncertainty in the mammalian phylogeny. First, we used the Bayesian methods implemented in Mr.Bayes version 3.1 (Ronquist and Huelsenbeck 2003; Huelsenbeck and Ronquist 2005) to construct Bayesian phylogenies based on the CFTR and mitochondrial sequence datasets. We specified a GTR model of molecular evolution with a gamma distribution of rates across four classes to generate the posterior probability distribution of CFTR phylogenies. A GTR model with a gamma distribution of rates across four classes and a proportion of invariant sites was used to generate the posterior distribution of mitochondrial trees. In both cases, two Monte Carlo Markov chains were simultaneously run for 250,000 generations, with sampling occurring every 100th generation following a 62,500 generation burn-in period. The consensus CFTR and mitochondrial trees were determined by a 50% majority rule criterion, but we retained all 3750 trees sampled from each posterior distribution for further analysis (see below). We also constructed trees using the neighbor joining and parsimony algorithms implemented in phylip version 3.66 (*neighbor* and *dnapars*) (Felsenstein 1989). The distance matrices input into phylip's neighbor program were constructed under Felsenstein's model of molecular evolution (Felsenstein and Churchill 1996) using *dnadist*. We adopted the default parameter settings in *neighbor* and *dnapars* to construct the trees, with the exception of specifying treatment of platypus as an outgroup. Nodal support on each tree was quantified with 1000 bootstrap replicates (see online Supplementary Fig. S1 A–D). As before, the platypus lineage was pruned from each phylogeny before deriving the corresponding variance–covariance matrix.

As a second approach to accounting for the effects of phylogenetic uncertainty, we considered the distribution of the H_P^2 of recombination across a number of independent bootstrap samples from the CFTR and mitochondrial datasets. We constructed an ML tree corresponding to each of 1000 bootstrap replicates from the CFTR sequence alignment using phyml, with the following evolutionary model features specified: GTR model with a gamma distribution of rates across four classes, gamma rate parameter estimated by likelihood, and ML estimates of nucleotide base frequencies. Similarly, we constructed ML phylogenies for each of 100 bootstrap replicates from the mitochondrial sequence alignment, assuming a GTR model with a gamma distribution of rates across four classes, a proportion of invariant sites, and ML estimates of base frequencies. Only 100 bootstrap replicates were considered from the mitochondrial alignment as the computing time required to infer the ML tree for each replicate was considerable owing to the large size of this dataset. We estimated the H_P^2 of recombination rate for each bootstrap replicate using the phylogenetic mixed model to derive a distribution of heritabilities realized from the empirical CFTR and mitochondrial sequence alignments. In a similar vein, we also computed the H_P^2 of recombination rate for each of the 3750 trees sampled from the posterior probability distribution of CFTR trees and each of the 3750 trees sampled from the posterior probability distribution of mitochondrial trees to derive approximations to the corresponding posterior distributions of H_P^2.

RANDOMIZATION TEST

The randomization test proposed by Freckleton and Harvey (2006) was performed to evaluate the Brownian assumption of homogeneity in the rate of evolution across the tree. Briefly, standardized phylogenetic contrasts were randomly permuted among the nodes of the mammalian phylogeny. Using established mathematical properties of Brownian motion, a phenotypic trait vector corresponding to the permuted arrangement of contrasts was derived, and the variance among these randomly generated recombination rates was computed. This procedure was iterated 10,000 times to generate an empirical distribution of variances expected under a Brownian motion model. The position of the observed variance along this distribution provides a measure of compliance to a Brownian motion model; the null hypothesis of neutral evolution is rejected if the observed variance lies in either tail of the distribution. We used an alpha value of 0.05 to assess significance.

ORNSTEIN–UHLENBECK MODEL

We fit Ornstein–Uhlenbeck (OU) models of stabilizing selection over the CFTR and mitochondrial ML mammalian phylogenies using the method of Hansen (1997) as implemented in the R package OUCH (Butler and King 2004). OU models present an elaboration to a Brownian motion model through the inclusion of additional parameters that specify an optimal trait value and the strength of selection toward the adaptive optimum. We considered four distinct cases and applied standard model selection procedures to discriminate among the evolutionary scenarios tested. First, we considered an OU model with no optimal trait value, a special case that reduces to Brownian motion. Second, we fitted a model with a single common trait optimum shared by all mammalian lineages. Finally, we considered a selective regime with a metatherian-specific adaptive optimum and one in which only the rodent lineage was governed by a distinct optimal rate of recombination. These models were selected to test whether the low rates of recombination in metatherian species and in rodents were likely to have arisen by evolutionary shifts in adaptive optima along these lineages. Models with additional parameters could not be tested with a dataset of this size ($n = 13$).

Results

VARIATION IN AVERAGE GENOMIC RECOMBINATION RATES AMONG MAMMALS

We measured average genomic recombination rates in 13 mammalian species by dividing the total sex-averaged genetic map length (in cM) of a given species by its physical genome size in Mb (Table 2). These genomic recombination rates are accompanied by large errors, as both genetic and physical map lengths are estimated with uncertainty. In particular, genetic map distances can be imprecise when the number of markers is small and when map coverage is incomplete, and map resolution is compromised when recombination fractions are inferred from few informative meiotic events.

Several genetic maps, like those for human and cow, are extremely high quality, whereas others are less complete. For example, several chromosomes are extremely marker poor or completely unrepresented on the cat genetic map, and the estimate of total genetic map length in this species is partially interpolated from cytological data (Menotti-Raymond et al. 1999). Additional trouble points include the limited number of informative meiotic events captured on the rat and mouse genetic maps and the relatively small pedigrees used to build the maps for horse and pig. The most recent dog genetic map does not include X chromosome data, and we use the sex-averaged X chromosome genetic map length from an earlier map. Few genetic markers were used to construct the metatherian maps, but independent cytological evidence corroborates the low genomic recombination rates revealed by genetic maps (Hayman et al. 1988; Sharp and Hayman 1988), and suggests that the addition of more markers would result in little expansion in map size.

Several patterns indicate that the substantial length variation among mammalian genetic maps reflects bona fide recombination rate differences between species rather than differences in map coverage and resolution (Table 2). First, there is a strong linear relationship between total genetic map length and the average number of chiasmata per male meiosis (Adjusted $R^2 = 0.86$, $P = 3.7 \times 10^{-6}$; solid line, Fig. 1), suggesting that estimates of genetic map length capture the amount of recombination per genome per meiosis with reasonable levels of precision. This solid linear model fit is particularly notable given that this regression line compares a measure of male recombination to a sex-averaged measure (and therefore provides a conservative estimate of the reliability of genetic maps). Furthermore, the regression line from the seven species with the most marker-dense genetic maps (rat, mouse, cow, pig, human, dog, and sheep; dashed-line, Fig. 1) provides a decent approximation to the relationship between chiasma count and total genetic map length in the remaining six species (filled circles, Fig. 1). Second, we detect no correlation between total genetic map length and marker number across the set of mammalian

Table 2. Average genomic recombination rates.

Species	Genetic map length (cM)[1]	Physical genome length (Mb)	Rate (cM/Mb)[1]	Natural log-transformed rate (cM/Mb)	Chakravarti et al. (1991) correction (cM/Mb)	Hall and Willis (2005) correction (cM/Mb)	Percent genome coverage[2]	Body weight (kg)[1,3]
Human	3615	3191	1.133	0.125	1.144	1.144	100	4.248
Baboon	2013	3100	0.649	−0.432	0.732	0.739	82.6	2.996
Macaque	2275	3100	0.734	−0.309	0.838	0.830	76.1	1.792
Mouse	1361	2600	0.523	−0.648	0.527	0.527	100	−3.912
Rat	1542	2800	0.551	−0.596	0.747	0.746	100	−1.204
Horse	2770	2700	1.026	0.026	1.128	1.122	93.1	6.273
Cat	3300	3000	1.100	0.095	1.348	1.295	53.5	1.386
Dog	3884	2500	1.554	0.441	1.604	1.603	99.9	2.996
Pig	2286	3000	0.762	−0.272	0.796	0.795	98.8	4.610
Sheep	3588	3000	1.196	0.178	1.260	1.258	94.5	5.298
Cow	3160	3000	1.053	0.052	1.070	1.070	100	6.620
Wallaby	829	3700	0.224	−1.496	0.309	0.291	53.8	1.386
Opossum	644	3500	0.184	−1.693	0.228	0.222	72.9	−2.303
CFTR	H_P^2=0.810	H_P^2=1.00	H_P^2=0.903	H_P^2=0.995	H_P^2=0.952	H_P^2=0.955	–	H_P^2=0.945
	P=0.041	P=0.001	P=0.0217	P=0.0187	P=0.0183	P=0.0161		P=0.0208
Mitochondria	H_P^2=1.00	H_P^2=1.00	H_P^2=0.996	H_P^2=0.998	H_P^2=0.995	H_P^2=0.993	–	H_P^2=0.998
	P=0.004	P=0.001	P=0.0083	P=0.0048	P=0.0072	P=0.0089		P=0.0050

[1] Sex-averaged.

[2] Percentage of the genome predicted to lie within 5 cM of a marker, assuming a random distribution of markers across the genome.

[3] Natural log transformed.

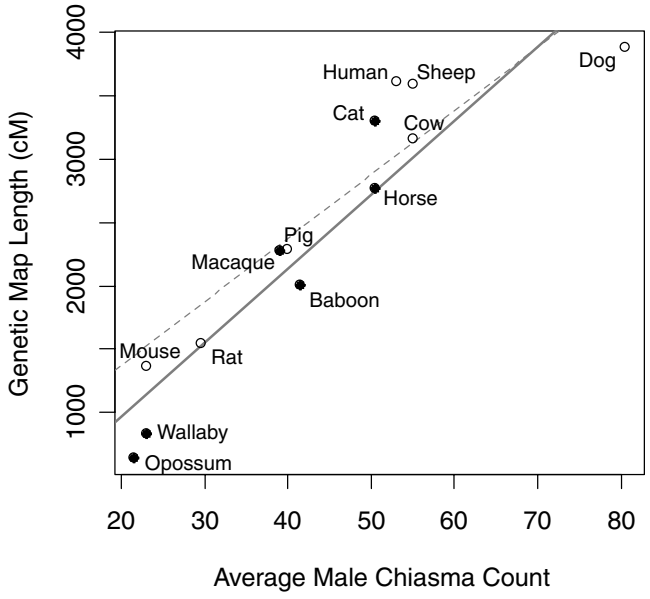

Figure 1. Relationship between total genetic map length and average male chiasma count. Simple linear regression of total genetic map lengths in centiMorgans units on the average number of chiasma at diplotene of meiosis I in males. The solid black line is a least squares linear model fit to all the datapoints ($y = 60.3x - 201.8$). The slope of this line is significantly nonzero ($P = 3.8 \times 10^{-6}$) and variation in male chiasma counts is well explained by variation in total genetic map lengths (Adjusted $R^2 = 0.85$). The dashed line is a least squares linear model that was fit to the seven species featuring the highest quality genetic maps (open circles: $y = 50.1x + 372.7$, Adjusted $R^2 = 0.85$). Species excluded in this partial regression are denoted by the filled circles.

maps (Spearman's $\rho = 0.38$, $P = 0.19$). A relationship between these variables is expected if variation in marker number is predictive of total genetic map length. Moreover, there is no correlation between the number of informative meiotic events and total genetic map length (Spearman's $\rho = 0.0056$, $P = 0.99$), indicating that differences in the resolution of these mammalian maps cannot explain the observed levels of variation among them. Finally, we calculated the expected genome coverage of each map given the total number of markers on the map (Hall and Willis 2005). For all species except cat and wallaby, at least 70% of the genome is predicted to lie within 5 cM of a marker on the genetic map (Table 2) and all the mammalian maps used in this analysis have at least 90% coverage at a distance of 15 cM. These coverage estimates are conservative, as they assume a random distribution of genetic markers. In reality, marker ascertainment schemes intentionally select loci that are overdispersed across the genome to maximize physical coverage. Taken together, these observations strongly suggest that the mammalian genetic maps used in this study accurately measure total amounts of recombination.

PHYLOGENETIC HERITABILITY OF MAMMALIAN RECOMBINATION RATES

At first glance, there appears to be some phylogenetic organization in the distribution of average genomic recombination rates in mammals (Table 2). Two trends are most prominent. First, the two metatherians (wallaby and opossum) have lower genomic average rates of recombination than any eutherian species, suggesting that the Methatheria–Eutheria split was accompanied by either a jump in the genomic average rate of recombination along the eutherian lineage or a reduction in rate along the lineage leading to metatherians. Second, within Eutheria, rodents display the lowest rates of recombination (Table 2). On the whole, it appears that more closely related species have more similar average rates of recombination (Fig. 2).

To test this hypothesis, we use Lynch's phylogenetic mixed model of quantitative trait evolution (Lynch 1991) to estimate the phylogenetic heritability (H_P^2) of the average genomic recombination rates. The H_P^2 of mammalian average genomic recombination rates along the nuclear CFTR phylogeny is 0.903 (Table 2) and this value lies in the 0.9783 quantile ($P = 0.0217$) of the distribution of 10,000 random H_P^2 values generated by permuting recombination rates across the tree tips (see Materials and Methods; Fig. 3A). Likewise, the H_P^2 of genomic recombination rates on the mitochondrial phylogeny is significant ($H_P^2 = 0.996$, $P = 0.0083$; Figure 3B). This signal is robust to removal of the rodent lineage ($H_P^2 = 0.879$, $P = 0.0350$ for the CFTR tree; $H_P^2 = 0.991$, $P = 0.0151$ for the mitochondrial tree), and also withstands exclusion of the metatherian clade ($H_P^2 = 0.872$, $P = 0.0217$ for the CFTR tree; $H_P^2 = 0.981$, $P = 0.0361$ for the mitochondrial tree).

The degree of phylogenetic relatedness is also an excellent predictor of total genetic map length unstandardized by genome size (CFTR: $H_P^2 = 0.810$, $P = 0.041$; Mitochondrial: $H_P^2 = 1.000$, $P = 0.004$; Table 2). Both the amount of recombination per se (as measured by cM) and the amount of recombination that occurs per unit of physical sequence (as measured by cM/Mb) are well predicted by the phylogenetic relationships among mammals.

A second independent measure of recombination, average male chiasma count, reproduces the strong phylogenetic signal observed with map-based estimates of recombination rate (CFTR Tree: $H_P^2 = 0.997$, $P = 0.0170$; Mitochondrial Tree: $H_P^2 = 0.999$, $P = 0.0046$; Table 3). In mammals, at least one chiasma per chromosome arm is necessary to ensure proper segregation of homologous chromosomes during meiosis (Dutrillaux 1986; Pardo-Manuel de Villena and Sapienza 2001). The number of chiasmata in excess of the number of chromosome arms provides a gauge of how much recombination occurs beyond this mechanistic requirement. The phylogenetic heritability of the number of chiasmata in excess of chromosome arms is also significant in mammals (CFTR Tree: $H_P^2 = 0.956$, $P = 0.0239$; Mitochondrial Tree: $H_P^2 = 0.997$, $P = 0.0201$; Table 3), implying that interspecific variation

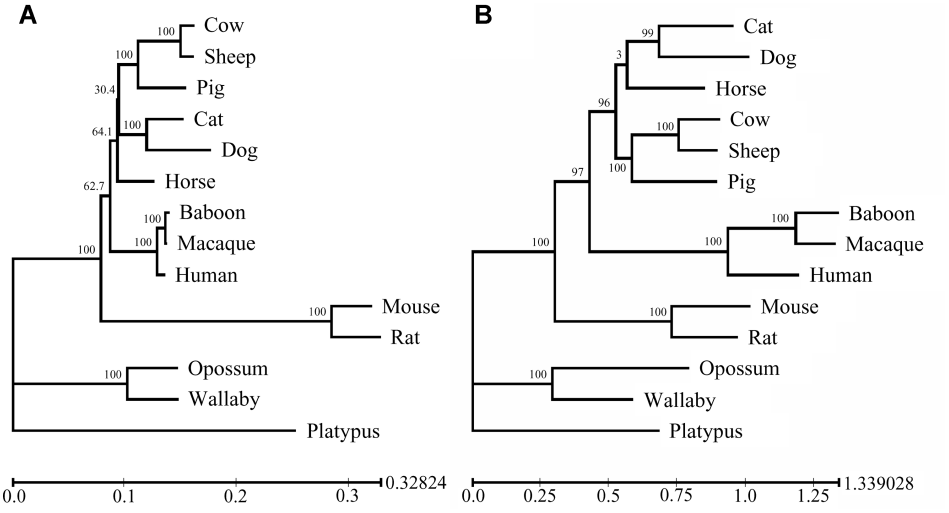

Figure 2. **Mammalian phylogenies. (A) Maximum-likelihood mammalian phylogeny based on CFTR coding sequences. The tree was constructed assuming a general time reversible model of molecular evolution with a gamma distribution of rates across four classes. Values at nodes represent the percentage of bootstrap replicates out of 1000 that support the clade. (B) Maximum likelihood tree based on concatenated mitochondrial coding sequences. The phylogeny was constructed under a general time reversible model of molecular evolution with a gamma distribution of rates across four classes and assumes a proportion of invariant sites. Nodal support is given as the percentage of bootstrap replicates ($n = 100$) that yield the clade.**

in the number of chromosome arms does not explain the signal we report.

EVALUATING MODEL ASSUMPTIONS AND EXPLORING SOURCES OF ERROR

The phylogenetic mixed model assumes that phenotypic values are normally distributed. Although we detected no deviation from normality in mammalian genomic recombination rates, it is difficult to evaluate the appropriateness of this assumption for a sample of size $n = 13$. Nevertheless, a log-transformation of the data increases the phylogenetic signal of mammalian recombination rates (CFTR Tree: $H_P^2 = 0.995$, $P = 0.0187$; Mitochondrial Tree: $H_P^2 = 0.998$, $P = 0.0048$; Table 2).

The phylogenetic mixed model further assumes that error associated with phenotypic measurement is randomly distributed with respect to the phylogeny. Recombination rate estimates are

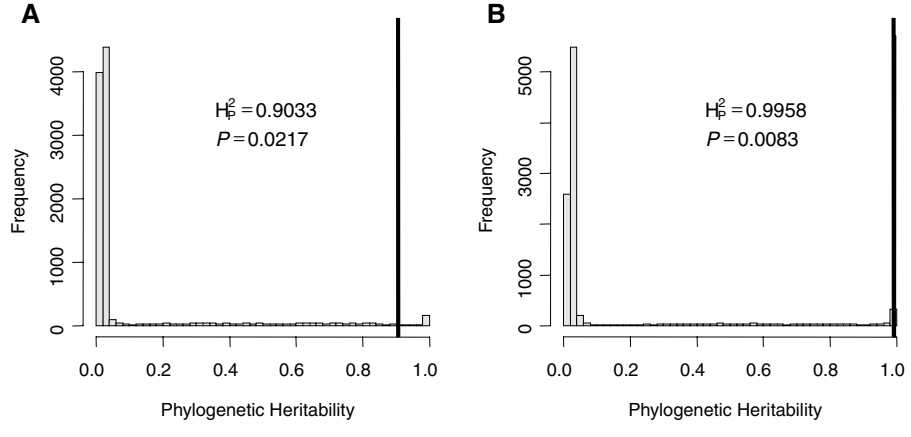

Figure 3. **Null distribution of phylogenetic heritability in mammalian recombination rates. Recombination rate values were randomly permuted with respect to species designations at tree tips and the H_P^2 of each pseudo-random replicate was estimated using the phylogenetic mixed model. In total, 10,000 permutations were conducted to generate the expected distribution of H_P^2 in mammalian average genomic recombination rates under the null hypothesis of no phylogenetic effect. Across the CFTR phylogeny, the observed H_P^2 (0.903) lies at the 0.9783 quantile of the distribution and is denoted by the vertical line (A). Along the mitochondrial tree, the H_P^2 of recombination rates is 0.996 (vertical black line), and this value lies at the 0.9917 quantile of the empirical distribution (B).**

Table 3. Average male chiasma counts per genome per meiosis.

Species	Haploid chromosome number	Number of chromosome arms/haploid genome	Average chiasma count	Chiasma in excess of the number of chromosome arms
Human	23	41	53[1]	12
Baboon	21	42	41.5[1]	−0.5
Macaque	22	42	39[1]	−3
Mouse	20	20	23[1]	3
Rat	21	33	29.5[1]	−3.5
Horse	32	41	50.5[1]	9.5
Cat	19	38	50.5[1]	12.5
Dog	39	39	80.5[1]	41.5
Pig	27	32	40[1]	8
Sheep	19	31	55[1]	24
Cow	30	31	55[1]	24
Wallaby	8	14	23[2]	9
Opossum	9	15	21.5[3,4]	6.5
CFTR	H_P^2=0.791	H_P^2=1.00	H_P^2=0.997	H_P^2=0.956
	P=0.0331	P=0.0015	P=0.0170	P=0.0239
Mitochondria	H_P^2=0.698	H_P^2=1.00	H_P^2=0.999	H_P^2=0.997
	P=0.0534	P=0.0015	P=0.0046	P=0.0201

[1] Burt and Bell 1987.
[2] Sharp and Hayman 1988.
[3] Hayman et al. 1988.
[4] Carvalho et al. 2002.

associated with large uncertainties, particularly when marker sampling is limited, but variation in marker number among mammalian genetic maps is not phylogenetically heritable (CFTR Tree: $H_P^2 = 0.0003$, $P = 0.256$; Mitochondrial Tree: $H_P^2 = 0.0003$, $P = 0.235$; Table 1). Rates of recombination inferred from chiasma number have lower sampling variances than genetic map-based rates (Broman et al. 2002), and we replicate a strong phylogenetic signal using this alternative measure. In addition, the signal is robust to the genetic map corrections proposed by Chakravarti et al. (1991) and Hall and Willis (2005) (Table 2).

Alternative genetic-map-based estimates of genomic recombination rates also reveal a significant phylogenetic trend. Substituting an estimate of the average rate of recombination in mouse inferred from a second genetic map still yields a high phylogenetic heritability ($H_P^2 = 0.894, P = 0.0228$ and $H_P^2 = 0.993, P = 0.0102$ for the CFTR and mitochondrial trees, respectively) (Shifman et al. 2006). Similarly, the estimate of H_P^2 is still quite high when the raw cat genetic map length (2040 cM) is used in place of the cytologically ameliorated estimate (CFTR: $H_P^2 = 0.809$, $P = 0.0319$; Mitochondrial: $H_P^2 = 0.962$, $P = 0.0346$), and also when the estimate of the total genetic map length for dog is taken from the earlier, marker poor map (1845 cM; CFTR: $H_P^2 = 0.796$, $P = 0.0394$; Mitochondrial: $H_P^2 = 0.987$, $P = 0.0208$) (Neff et al. 1999). Joint consideration of these three alternative estimates of average recombination rate still yields a high heritability ($H_P^2 = 0.772$, $P = 0.0391$ and $H_P^2 = 0.988$, $P = 0.0194$ for the CFTR and mitochondrial trees, respectively). Overall, the phylogenetic signal appears to be surprisingly robust to error in genomic recombination rate estimates.

A third assumption of the phylogenetic mixed model is that the underlying phylogeny is known without error. The phylogeny of mammals remains unresolved, but much of the uncertainty concerns the placement of short branches that contribute minimally to the covariance between species (Springer et al. 2004). Accounting for this uncertainty is therefore not likely to qualitatively change the pattern that emerges from the phylogenetic distribution of mammalian recombination rates, but we nonetheless take several measures to assess its impact on the signal we report.

First, we jointly consider mammalian trees constructed from the nuclear CFTR locus and mitochondrial sequence data. Analyses based on these two trees corroborate nicely, effectively dismissing the possibility that the signal is produced by evolutionary processes specific to either sector of the genome. Second, the CFTR and mitochondrial ML trees recovered under different models of molecular evolution all yield high estimates of H_P^2 in recombination rate, ruling out evolutionary model choice as a conflating factor (Range of CFTR $H_P^2 = 0.902$–0.911; see online Supplementary Table S2; Range of mitochondrial $H_P^2 = 0.987$–0.995; see online Supplementary Table S3). Third, average genomic recombination rates are still phylogenetically distributed

Table 4. Phylogenetic heritability of genomic average recombination rate on Bayesian, parsimony, and neighbor-joining (NJ) trees.

Method of phylogeny construction	Locus	Phylogenetic heritability of recombination rate	*P*-value
NJ	CFTR	0.9096	0.0301
	Mitochondrial	0.9866	0.0116
Parsimony	CFTR	0.8914	0.0255
	Mitochondrial	0.9886	0.0121
Bayesian	CFTR	0.9085	0.0220
	Mitochondrial	0.9926	0.0104

along trees built using Bayesian, neighbor joining, and parsimony approaches to phylogeny construction (Table 4). Fourth, we generated ML trees for 1000 bootstrap sequence samples drawn from the CFTR sequence alignment and 100 bootstrap sequence samples drawn from the mitochondrial dataset. We measured the phylogenetic heritability of recombination rate on each bootstrap tree to generate a distribution of heritabilities realized from the empirical sequence datasets (Figs. 4A and 4B). The distribution of H_P^2 on the CFTR phylogeny is centered on 0.907, and the corresponding 95% confidence interval is quite narrow (0.865–0.993), suggesting that phylogenetic uncertainty has a small effect on the observed signal (Fig. 4A). We document a similar pattern on the mitochondrial tree (mean = 0.992, 95% CI = 0.991–0.996; Fig. 4B). Finally, the distributions of recombination rate H_P^2 along trees sampled from the Bayesian posterior probability distributions of CFTR and mitochondrial phylogenies are confined to narrow intervals (CFTR 95% CI = 0.867 – 0.992; Mitochondrial 95% CI = 0.990–0.997; Fig. 4C and D).

The small size of the sequence datasets we used to construct the mammalian tree and the incomplete nature of our taxon sampling likely explain the inconsistencies between our trees and previously published mammalian phylogenies. First, the two ML

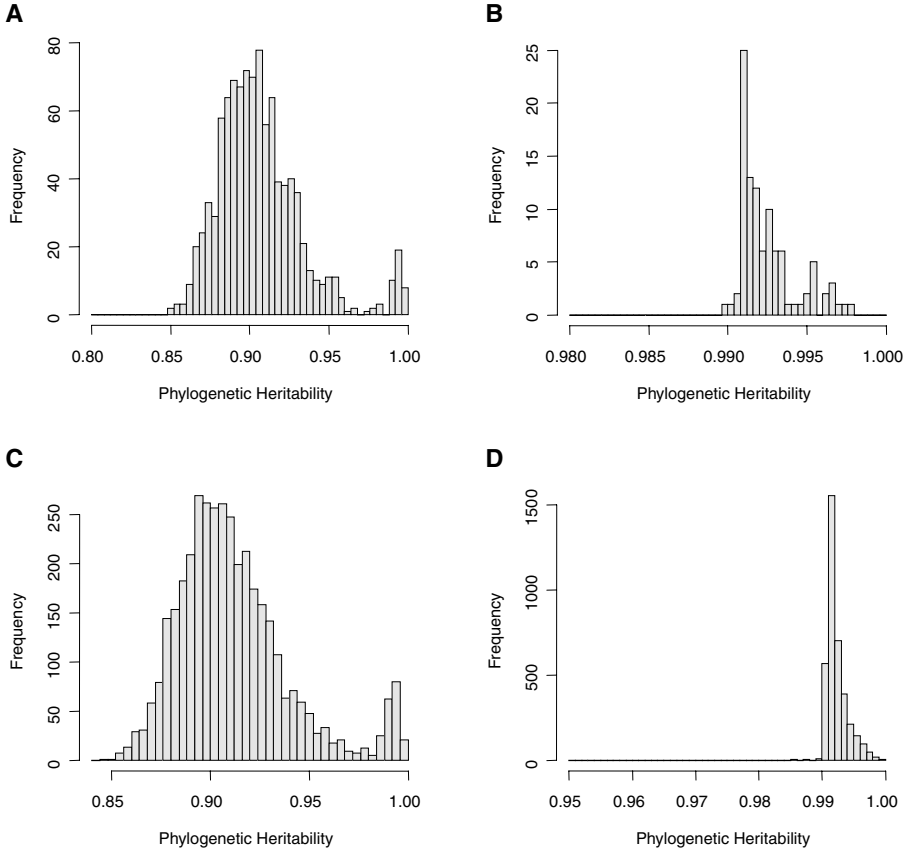

Figure 4. Distribution of phylogenetic heritabilities across alternative trees. Additional sequence datasets were generated by bootstrap sampling from the empirical CFTR and mitochondrial multiple sequence alignments (A and B). A maximum-likelihood phylogenetic tree was constructed for each bootstrap replicate, and the heritability of recombination rate on each tree estimated using the phylogenetic mixed model. Panel (A) shows the distribution of heritabilities across 1000 CFTR phylogenies and (B) is the distribution of phylogenetic heritabilities over 100 alternative phylogenies generated by bootstrap sampling from the mitochondrial sequence alignment. The phylogenetic heritability of average genomic recombination rates was also estimated along 3750 trees sampled from the Bayesian posterior distribution of CFTR (C) and mitochondrial (D) phylogenies.

trees we recover do not capture the well-accepted sister relationship between primates and rodents (Murphy et al. 2001b; Waddell et al. 2001; Springer et al. 2004; Kriegs et al. 2006; Figure 2), but instead place rodents as a basal Eutherian lineage. Second, the CFTR-based ML tree places horse as ancestral to both artiodactyls and carnivores, rather than sister to carnivores (Xu et al. 1996; Lin et al. 2002). Despite these two inconsistencies, the trees used in this analysis are largely congruent with previous reconstructions of the mammalian phylogeny based on larger datasets, denser taxon sampling, and more sophisticated approaches of phylogeny construction (Madsen et al. 2001; Murphy et al. 2001a; Lin et al. 2002; Kriegs et al. 2006). Moreover, none of the nodes supporting these "misplaced" clades are supported by 100% of bootstrap replicates on our phylogenies, and our analyses of each independent bootstrapped sequence dataset effectively dismiss the possibility that alternative topological arrangements yield a weak phylogenetic signal. The inclusion of additional mammalian taxa (armadillo, elephant, rabbit, and guinea pig for the CFTR tree; an additional 21 species for the mitochondrial tree) in phylogeny reconstruction had little impact on the relative branch lengths and the topological relationships among the 13 species of interest, suggesting that our trees are not biased by restricted taxon sampling. The removal of branches featuring species without recombination rate data from these taxon-rich phylogenies, and the subsequent estimation of genomic recombination rate H_P^2 along these pruned trees still yielded strong phylogenetic signals (CFTR: $H_P^2 = 0.913$, $P = 0.0222$; Mitochondrial: $H_P^2 = 0.994$, $P = 0.0137$). Lastly, ML trees constructed with an a priori specification of the accepted mammalian topology still bear a high H_P^2 of genomic recombination rates (CFTR: $H_P^2 = 0.921$, $P = 0.0224$; Mitochondrial: $H_P^2 = 0.993$, $P = 0.0505$).

HOMOGENEITY IN THE TEMPO OF RECOMBINATION RATE EVOLUTION IN MAMMALS

The strong phylogenetic signal detected using the phylogenetic mixed model indicates that the evolution of average genomic recombination rate is well approximated by a Brownian motion model. Good compliance with this model may imply that the evolution of mammalian average rates of recombination is neutral, but processes such as rapid fluctuating directional selection may mimic the phylogenetic variance–covariance structure produced by a Brownian process (Freckleton and Harvey 2006; O'Meara et al. 2006). If the evolution of mammalian recombination rates is neutral, and the distribution of mutational effects is similar across species, the rate of evolution should be constant across the phylogeny. We directly test this prediction using a simple randomization test (see Materials and Methods).

We compare the observed variance in genomic average rates of recombination to the distribution of trait variances from 10,000 pseudo-replicated samples on the CFTR and mitochondrial phylogenies. The observed variance lies in the 46.86 percentile of the empirical trait variance distribution from the CFTR tree and at the 90.86 percentile of the distribution derived from the mitochondrial phylogeny (Fig. 5). The variance in mammalian recombination rates is within the range of that expected under Brownian motion along both trees. By this test, we fail to find evidence for

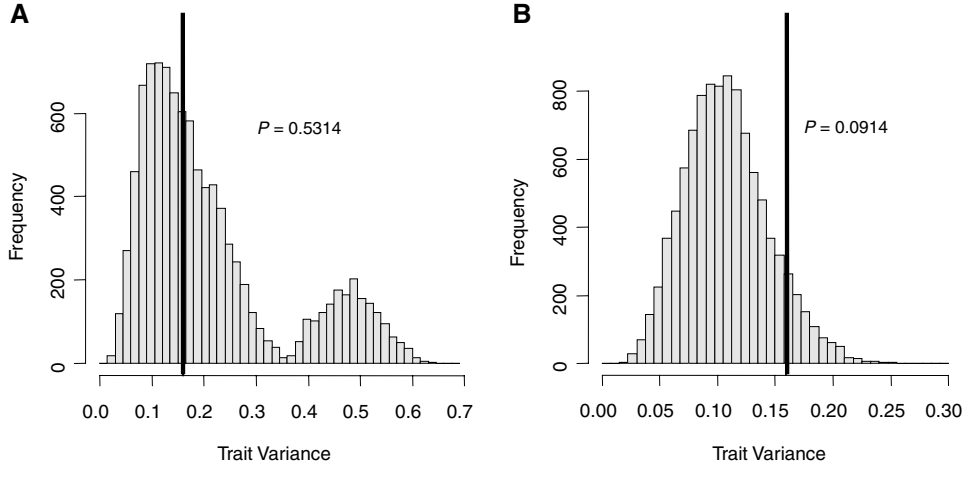

Figure 5. Distribution of simulated trait variances. Observed phylogenetic independent contrasts were randomized across the mammalian tree and properties of Brownian motion were applied to generate phenotypic trait values corresponding to the permuted arrangement of contrasts. We measure the trait variance associated with each of 10,000 randomized datasets to generate the empirical distribution of variance in genomic average recombination rates. Across the CFTR phylogeny, the observed trait variance is within the range of randomly generated trait variances (Observed = 0.16, Quantile = 0.4686) and is denoted by the vertical line (A). Similarly, along the mitochondrial phylogeny, the observed trait variance (0.16, vertical black line) is not extreme relative to the empirical distribution of trait variances (Quantile = 0.9086) (B).

heterogeneity in the rate of evolution in recombination rates across the various lineages of the mammalian phylogeny.

NONNEUTRAL MODELS OF QUANTITATIVE TRAIT EVOLUTION

We impose four unique OU models of stabilizing selection onto the CFTR mammalian phylogeny to determine whether alternative evolutionary scenarios are likely to have given rise to the observed phylogenetic distribution of recombination rates in mammals. ML estimates of the model parameters for each selective regime tested are given in Table 5. First, we fit a simple Brownian motion model and compute the maximum likelihood of the data under this neutral regime for comparison to alternative models of stabilizing selection. Next, we apply a model with a single global trait optimum. The estimate of the optimal genomic recombination rate in mammals, θ_a, is hugely negative in this case ($\theta_a = -1.70 \times 10^8$), suggesting that either our sample of 13 species is insufficient for testing parameter rich models or that the algorithm for estimating model parameters is prone to converge on local maxima in the likelihood surface. This model does not present a significantly better fit to the data than the simple Brownian motion case, as assessed by the Akaike information criteria and a likelihood ratio test ($\chi^2 = 1.18$, df $= 2$, $P = 0.55$). The third model considers a separate optimum value in metatherians, whereas an individual optimum is specified for the lineage leading to rodents in the fourth model. The third model provides a significantly better fit to the data than does the nested Brownian motion case ($\chi^2 = 18.59$, df $= 3$, $P = 0.0003$), but yields unrealistic estimates of several model parameters (Table 5). The large number of parameters to be estimated from a sample size of 13 urges that these results be interpreted with caution (Hansen 1997). A likelihood ratio test shows that the fourth model is also preferable to the basic Brownian motion model ($\chi^2 = 8.46$, df $= 3$, $P = 0.037$), but according to the AIC, the Brownian motion model is preferred (Table 5). This discrepancy highlights the tenuous nature of these results and the statistical challenge of estimating a large number of parameters from a small amount of data. In particular, the estimate of the ancestral recombination rate at the ancestral node on the phylogeny is negative, a biologically impossible observation (Table 5).

We fit the same four OU models on the mitochondrial phylogeny and observe similar trends. A Brownian motion model is preferable over the three more parameter-rich models as assessed by the AIC, but a likelihood ratio test indicates that the model with a distinct evolutionary regime in Metatheria provides a better fit to the data ($\chi^2 = 8.62$, df $= 3$, $P = 0.035$; Table 5). Again, however, we note that the ML estimates of lineage-specific recombination rate optima are negative, suggesting that the model performs poorly on small datasets and/or that the likelihood surface is especially rugged.

Discussion

PHYLOGENETIC SIGNAL OF GENOMIC AVERAGE RECOMBINATION RATES

Our application of phylogenetic comparative methods demonstrates that more closely related mammals have more similar sex-average rates of recombination. This phylogenetic signal is strong across the mammalian tree, on par with that of log-transformed body mass (Table 2). The latter phenotype is an especially well-studied trait in mammalian evolution, and is frequently cited as an example of a quantitative character exhibiting a clear phylogenetic signature (Smith et al. 2004). The strong signal in mammalian average genomic recombination rates persists in spite of errors in estimates of genetic map lengths, and is robust across a number of alternative tree topologies, branch lengths, and phylogenetic model choices (Fig. 4; see online Supplementary Tables S2 and S3; Fig. S1). In fact, all measurement error, phylogenetic uncertainty, and error due to poor model fit are accounted for in the $1 - H_P^2$ term. For genomic sex-average recombination rates, this quantity is small (0.0967 and 0.0042 for the CFTR and mitochondrial based H_P^2 estimates).

The strong phylogenetic signal in sex-averaged mammalian recombination rates is recapitulated using a second independent metric of recombination, average male chiasma counts. The phylogenetic heritability of this measure is higher than that of sex-averaged recombination rates measured from genetic maps, a result that is likely a consequence of two distinct phenomena. First, because only two of the four chromatids involved in a crossover exchange at meiosis bear recombinant genotypes, recombination fractions inferred from patterns of genetic inheritance in pedigrees or crosses are impacted by binomial sampling error. Chiasma counts are direct cytological observations of recombination events, and are consequently not affected by error induced by the sampling of recombinant chromosomes. Second, many mammalian species show a striking sexual dimorphism in recombination rates, which casts some doubt on the biological meaning of a sex-averaged rate. The stronger phylogenetic signal in male chiasma counts may be tethered to the more tractable genetic basis of this measure. The presence of a striking sex difference clearly motivates evolutionary analyses of sex-specific recombination rate evolution (Lenormand 2003), but few sex-specific genetic maps are currently available in mammals and the temporal aspects of oogenesis render female chiasma counts challenging to obtain.

Although two distinct measures of recombination agree in their detection of a prominent phylogenetic signature, our analysis may be underpowered to detect the absence of a signal. However, we contend that this possibility is unlikely for several reasons. Our nonparameteric approach for computing P-values involves the permutation of recombination rates at the tips of the mammalian phylogeny followed by the estimation of the H_P^2 on the permuted dataset. We fail to find a high phylogenetic heritability for most

Table 5. Ornstein–Uhlenbeck models of stabilizing selection.

Tree	Regime	α[1] $(\text{years})^{-1}$	σ^2[2] $(\frac{d(cM/Mb)}{dt})^2$	θ[3] (cM/Mb)	θ_a[4] (cM/Mb)	θ_m[5] (cM/Mb)	θ_r[6] (cM/Mb)	$-2\times\ln(\text{lik})$	df	AIC	LRT[7]
CFTR	Brownian motion	–	0.63	0.69	–	–	–	6.97	2	10.97	–
	Single optimum in mammals	7.98×10^{-9}	0.62	0.91	-1.70×10^{8}	–	–	6.38	4	14.38	χ^2_2=1.18
	Metatherian-specific optimum	30.27	1.72	21100	−0.53	−198.5	–	−2.33	5	7.67	χ^2_3=18.59**
	Rodent-specific optimum	1.29×10^{-7}	0.53	−0.86	8.33×10^{7}	–	1.17×10^{7}	2.74	5	12.74	χ^2_3=8.46*
Mitochondria	Brownian motion	–	0.32	0.62	–	–	–	6.68	2	10.68	–
	Single optimum in mammals	1.19×10^{-8}	0.32	0.42	1.98×10^{7}	–	–	6.53	4	14.53	χ^2_2=0.29
	Metatherian-specific optimum	0.5703	0.3503	2.4308	−0.6507	−3.9829	–	2.3704	5	12.37	χ^2_3=8.62*
	Rodent-specific optimum	4.12×10^{-9}	0.3086	0.4198	7.31×10^{7}	–	-4.60×10^{-7}	5.3646	5	15.36	χ^2_3=2.63

df, degrees of freedom; AIC, Akaike Information Criterion; *$P < 0.05$; **$P < 0.001$.

[1] The strength of the directional force toward the optimal trait value. The amount of time required to move halfway to the adaptive optimum is equal to $\ln(2)/\alpha$.

[2] The magnitude of random perturbations tolerated about the trait optimum.

[3] Maximum-likelihood estimate of the genomic recombination rate at the most ancestral node (root).

[4] Maximum-likelihood estimate of the optimal recombination rate across the mammalian tree.

[5] Maximum-likelihood estimate of the optimal recombination rate on the methatherian lineage.

[6] Maximum-likelihood estimate of the optimal recombination rate on the rodent lineage.

[7] χ^2 statistic from a likelihood ratio test with the Brownian motion model. The subscript on χ^2 specifies the degrees of freedom in the test.

randomized datasets (Fig. 3), suggesting that 13 species provide sufficient power to reject the hypothesis of a phylogenetic signal. Additionally, we do not detect a phylogenetic signature in the number of markers on the genetic maps of each species (Table 1), further confirmation that our sample size is large enough to detect aphylogenetic trends. Finally, the distribution of recombination rates among mammals is clearly organized in a nonrandom fashion with respect to phylogeny. The two metatherian species have the lowest rates of recombination among the species considered, and within Eutheria, rodents have the lowest rates (Tables 1 and 2). Based on visually discernable patterns, it is not surprising that we observe a phylogenetic signal.

The strong phylogenetic signal in mammalian genomic average recombination rates suggests that the total amount of recombination per meiosis in one species can provide a reliable prediction of the average genomic rate of recombination in a second species for which genetic maps are unavailable. This predictive power will be highest over short phylogenetic distances. For example, we might expect the chimpanzee (for which no genetic map is currently available) to have a similar average genomic rate of recombination to human. Building genetic maps for additional mammalian species—particularly species from clades distantly related to those sampled in this analysis (e.g., monotremes, bats, afrotherians, insectivores, and xenartherians)—would be useful for increasing predictive power across the full breadth of the mammalian phylogeny and for further refining the evolutionary pattern documented here.

ALTERNATIVE EXPLANATIONS FOR THE PHYLOGENETIC SIGNAL IN MAMMALIAN RECOMBINATION RATES

The phylogenetic signal in mammalian recombination rates could be due to the evolution of recombination per se or could represent a correlated evolutionary response to a distinct genomic or life-history trait. For example, recombination rates are not independent of the number of chromosome arms in a genome (Dutrillaux 1986; Pardo-Manuel de Villena and Sapienza 2001), and the pattern we document could be a correlated evolutionary response to changes in chromosome number and structure during mammalian evolution. However, our phylogenetic analyses of the number of chaisma per male genome in excess of the number of chromosome arms demonstrate that the amount of recombination in excess of fundamental requirements is still phylogenetically distributed in mammals (Table 3).

Relative to their wild progenitors and nondomesticated species, domesticated plants and animals tend to show elevated rates of recombination (Burt and Bell 1987; Ross-Ibarra 2004). Many of the mammalian species used in this analysis are domesticated, and the possibility remains that the phylogenetic pattern we detect is simply tracking differences in the domestication status of different species. However, several trends argue against this. First, humans are a nondomesticated species, yet display one of the highest mammalian recombination rates. Alternatively, opossum has been adapted to the laboratory environment, but has the lowest rate of recombination among the species considered. Although we cannot wholly dismiss the possibility, it appears unlikely that the phylogenetic signal we report is solely driven by recombination rate changes coincidental with domestication. Recombination rate data from the wild ancestors of domesticated mammalian species are currently unavailable, but would be useful for a test of this alternative explanation (Ross-Ibarra 2004).

THE EVOLUTION OF MAMMALIAN RECOMBINATION RATES MEASURED ON DIFFERENT PHYSICAL SCALES

The marked phylogenetic pattern we have documented in genomic recombination rates contrasts with expectations for fine-scale recombination rates. The fine-scale recombination landscape in mammals may be modulated primarily by recombination hotspots—small 1–2 kb regions of elevated recombination rate scattered at roughly 50-kb intervals across the genome—that are poorly conserved between closely related species (Ptak et al. 2004, 2005; Winckler et al. 2005). Similarly, recombination rates measured across 5 Mb orthologous genomic regions in human, mouse, and rat are only weakly positively correlated in pairwise comparisons (Jensen-Seaman et al. 2004), and rates of recombination measured in chicken and a passerine bird show no significant conservation at the megabase scale (Dawson et al. 2007).

The discrepant levels of conservation in recombination rates measured on different physical scales suggest that unique sets of evolutionary pressures operate at these different levels (Myers et al. 2005; Coop and Przeworski 2007). It is known that rates of recombination measured at the genome and chromosomal level are constrained by the necessity of crossing over for proper homolog disjunction at meiosis, whereas the rapid evolutionary dynamics of recombination hotspots appear to be largely driven by biased gene conversion away from the recombinationally active allele (Boulton et al. 1997). However, the connection between rates of recombination measured in individual recombination hotspots and broader-scale recombination rates has yet to be elucidated and presents a challenging focus for further investigations.

Although many recombination events do appear to concentrate to clearly defined hotspots, the true proportion of recombination events that occur in these regions (relative to intervening background sequence) is not known (but see Myers et al. 2005 for an estimate of this fraction inferred from patterns of linkage disequilibrium in the human genome). If a substantial proportion of recombination events does not occur in recombination hotspots but instead takes place in intervening background sequence, the rapid evolutionary dynamics of hotspots could be largely irrelevant to evolution of genomic scale recombination rates. On the

other hand, the extinction of one hotspot could heighten the intensity of neighboring hotspot loci or permit the birth of a new hotspot locus in an adjacent region, with the net effect of little to no change in the recombination fraction of a genomic interval (Myers et al. 2005). Similar phenomena have been described in yeast (Wu and Lichten 1995; Fan et al. 1997), and these processes may also operate to conserve broad-scale rates of recombination in mammals (Myers et al. 2005).

NEUTRAL EVOLUTION OF GENOMIC AVERAGE RECOMBINATION RATES

The distribution of average genomic recombination rates in mammals is well predicted by a Brownian motion model, suggesting that the evolution of average genomic recombination rates has been largely neutral on this time scale. Although non-neutral processes, such as rapidly fluctuating directional selection, can also produce patterns consistent with Brownian motion (Freckleton and Harvey 2006; O'Meara et al. 2006), we favor a neutral interpretation for several reasons. First, the phylogenetic heritability for recombination rates is high, leaving little room for model error. We would expect a neutral Brownian motion model to present a poor fit to the data if observed rates of recombination were instead realized under a selective scenario. Second, phylogenetic independent contrasts are randomly distributed across the mammalian topology, implying constancy of the evolutionary rate of recombination rate. Finally, alternative evolutionary models poorly describe the phylogenetic distribution of mammalian recombination rates. A Brownian motion model is statistically favored over several simple models of stabilizing selection, although results from these analyses are challenging to interpret and our small sample size limits power to test more complicated selective regimes. Even though we cannot rule out the possibility that this analysis is underpowered to detect departures from neutral evolution, results from multiple independent approaches fail to conclusively reject a simple neutral explanation for interspecific variation in genomic average recombination rates.

RECONCILING NEUTRAL EVOLUTION WITH KNOWN EVOLUTIONARY CONSTRAINTS

A number of previous studies have concluded that rates of recombination may be under strong selective constraints (Hulten 1974; Dutrillaux 1986; Pardo-Manuel de Villena and Sapienza 2001). Proper homologue disjunction at meiosis requires at least one chiasma per chromosome arm (Mather 1938), but too much recombination may build strong adhesive forces between chromosomes, inhibiting their separation and migration to opposite poles at anaphase I. Excessively high rates of recombination may also foster an environment conducive to nonhomologous recombination, leading to large-scale chromosomal alterations and widespread genomic instability. Rates of recombination should experience rigid selective pressures to fall above the minimum for correct segregation at meiosis, but below the threshold that presents an assault on genome integrity (Coop and Przeworski 2007). Indeed, aberrantly high or low rates of recombination are positively associated with increased levels of aneuploidy and decreased fecundity (Kidwell 1972; Micic et al. 1982; Koehler et al. 1996), and there is a remarkably uniform number of chiasmata per chromosome arm across a wide range of eukaryotic species (Pardo-Manuel de Villena and Sapienza 2001).

We propose that rates of recombination evolve neutrally within the bounds defined by the requirements for proper meiotic segregation and the maintenance of genome integrity. As rates of recombination drift toward either extreme, directional selective pressures act to push them back into the neutral range. Thus, the average probability of fixation of a mutation affecting recombination rates will be $1/2N_e$ within the bounded rate interval, but will be considerably higher or lower near the boundaries, depending on the mutation's effect size and the directionality of its effect. Consistent with this model of genomic recombination rate evolution, we find that the number of chiasma in excess of fundamental requirements presents a good fit to a Brownian motion model (Table 3), and appears to be neutrally evolving. A formal test of this model, however, will require identifying species situated at the minimum or maximum recombination rate boundary and asking whether they experience more rigid evolutionary restrictions.

Most of the mammalian species in this investigation are above the minimal threshold (Table 3), but their placement in relation to the upper bound remains undetermined. The biological constraints that define this upper limit are poorly characterized, but it is evident that rates of recombination can be quite high and still not impose a meiotic threat. The average genomic rate of recombination in the yeast *S. cerevisiae* is over two orders of magnitude greater than the average rate in humans (Cherry et al. 1997; Broman et al. 1998; Kong et al. 2002), and the average recombination rate in the honey bee is more than 10× higher than the rate in any mammalian species (Beye et al. 2006). Based on these observations, we speculate that most of the mammalian species considered in this analysis lie within the putatively neutral recombination rate region defined by the upper and lower boundaries.

QUANTITATIVE GENETIC PROSPECTS FOR RECOMBINATION RATE EVOLUTION

Although our analysis has focused on differences in recombination rates between species, there is also substantial polymorphism for both global and fine-scale rates of recombination within populations (Chinnici 1971; Brooks and Marks 1986; Broman et al. 1998; Kong et al. 2004; Samollow et al. 2004; Neumann and Jeffreys 2006). Studies in *Drosophila* have shown that this variation responds rapidly and smoothly to laboratory-imposed selective pressures, indicating the presence of abundant heritable variation for

recombination (Chinnici 1971; Kidwell 1972; Brooks and Marks 1986). Similarly, domesticated plants and mammals tend to have higher rates of recombination relative to their wild progenitors and other nondomesticated species (Burt and Bell 1987; Ross-Ibarra 2004), raising the possibility that loci of economic and agricultural importance are often tightly linked to modifiers of recombination rate. The complex genetic architecture of recombination implied by these studies, coupled with our finding that average genomic rates of recombination appear to evolve neutrally, suggest that species differences in recombination are predominantly due to the accumulation of neutral mutations across many loci.

This finding sets the stage for further application of quantitative genetics theory to the evolution of mammalian recombination rates. If average genomic rates of recombination evolve neutrally, levels of intraspecific polymorphism should be approximately equal to $2N_eV_m$ at equilibrium (if most mutations behave additively), where N_e is the effective population size and V_m is the rate at which variance in recombination rate accumulates via neutral mutations (Lynch and Hill 1986). This relationship suggests a simple test of neutral evolution in recombination rates: the amount of polymorphism in this trait should scale linearly with effective population size under neutrality (Lynch and Hill 1986). Testing this prediction would be useful for confirming the pattern we document here, but hinges on the development of improved metrics for quantifying intraspecific levels of recombination rate variation. Investigating the genetic basis of recombination rate polymorphism and divergence—in particular, determining the number of loci that have contributed to within and between species differences and the distribution of effect sizes—represents a critical first step in this direction and will provide additional clues about the evolutionary dynamics of this fundamental genetic trait.

ACKNOWLEDGMENTS

We thank C. Ané, K. Broman, A. Peters, S. Smith, and M. White for useful discussions and advice. We thank C. Ané, K. Broman, J. True, and two anonymous reviewers for providing constructive comments on earlier versions of this manuscript. This research was supported by a NIH Graduate Training Grant to the Laboratory of Genetics and a NSF Graduate Research Fellowship to BLD.

LITERATURE CITED

Barton, N. H. 1995. A general model for the evolution of recombination. Genet. Res. 65:199–221.

Baudat, F., and B. de Massy. 2007. *Cis*- and *trans*- acting elements regulate the mouse *Psmb9* meiotic recombination hotspot. PLoS Genet. 3:1029–1039.

Beye, M., I. Gattermeier, M. Hasselmann, T. Gempe, M. Schioett, J. F. Baines, D. Schlipalius, F. Mougel, C. Emore, O. Rueppell, et al. 2006. Exceptionally high levels of recombination across the honey bee genome. Genome Res. 16:1339–1344.

Boulton, A., R. S. Myers, and R. J. Redfield. 1997. The hotspot conversion paradox and the evolution of meiotic recombination. Proc. Natl. Acad. Sci. USA 94:8058–8063.

Broman, K. W., J. C. Murray, V. C. Sheffield, R. L. White, and J. L. Weber. 1998. Comprehensive human genetic maps: individual and sex-specific variation in recombination. Am. J. Hum. Genet. 63:861–869.

Broman, K. W., L. B. Rowe, G. A. Churchill, and K. Paigen. 2002. Crossover interference in the mouse. Genetics 160:1123–1131.

Brooks, L. D., and R. W. Marks. 1986. The organization of genetic variation for recombination in *Drosophila melanogaster*. Genetics 114:525–547.

Burt, A. 2000. Perspective: sex, recombination, and the efficacy of selection—Was Weismann right? Evolution 54:337–351.

Burt, A., and G. Bell. 1987. Mammalian chiasma frequencies as a test of 2 theories of recombination. Nature 326:803–805.

Butler, M. A., and A. A. King. 2004. Phylogenetic comparative analysis: a modeling approach for adaptive evolution. Am. Nat. 164:683–695.

Carvalho, B. D., L. F. B. Oliveira, A. P. Nunes, and M. S. Mattevi. 2002. Karyotypes of nineteen marsupial species from Brazil. J. Mammal. 83:58–70.

Chakravarti, A., L. K. Lasher, and J. E. Reefer. 1991. A maximum-likelihood method for estimating genome length using genetic linkage data. Genetics 128:175–182.

Charlesworth, B. 1976. Recombination modification in a fluctuating environment. Genetics 83:181–195.

Charlesworth, B., M. T. Morgan, and D. Charlesworth. 1993. The effect of deleterious mutations on neutral molecular variation. Genetics 134:1289–1303.

Cherry, J. M., C. Ball, S. Weng, G. Juvik, R. Schmidt, C. Adler, B. Dunn, S. Dwight, L. Riles, R. K. Mortimer, et al. 1997. Genetic and physical maps of *Saccharomyces cerevisiae*. Nature 387:67–73.

Chinnici, J. P. 1971. Modification of recombination frequency in *Drosophila*. II. Polygenic control of crossing over. Genetics 69:85–96.

Coop, G., and M. Przeworski. 2007. An evolutionary view of human recombination. Nat. Rev. Genet. 8:23–34.

Crow, J. F., and M. Kimura. 1965. Evolution in sexual and asexual populations. Am. Nat. 99:439–450.

Dawson, D. A., M. Åkesson, T. Burke, J. M. Pemberton, J. Slate, and B. Hansson. 2007. Gene order and recombination rate in homologous chromosome regions of the chicken and a passerine bird. Mol. Biol. Evol. 24:1537–1552.

Detlefson, J. A., and E. Roberts. 1921. Studies on crossing over. I. The effect of selection on crossover values. J. Exp. Zool. 32:333–354.

Dietrich, W. F., J. Miller, R. Steen, M. A. Merchant, D. Damron-Boles, Z. Husain, R. Dredge, M. J. Daly, K. A. Ingalls, T. J. O'Connor, et al. 1996. A comprehensive genetic map of the mouse genome. Nature 380:149–152.

Dutrillaux, B. 1986. Le rôle des chromosomes dans l'évolution: une nouvelle interprétation. Ann. Genet. 29:69–75.

Fan, Q. Q., F. Xu, M. A. White, and T. D. Petes. 1997. Competition between adjacent meiotic recombination hotspots in the yeast *Saccharomyces cerevisiae*. Genetics 145:661–670.

Felsenstein, J. 1974. The evolutionary advantage of recombination. Genetics 78:737–756.

———. 1989. PHYLIP - Phylogeny inference package (Version 3.2). Cladistics 5:164–166.

Felsenstein, J., and G. A. Churchill. 1996. A hidden Markov model approach to variation among sites in rate of evolution. Mol. Biol. Evol. 13:93–104.

Fisher, R. A. 1930. The genetical theory of natural selection. Oxford Univ. Press, London.

Freckleton, R. P., and P. H. Harvey. 2006. Detecting non-Brownian trait evolution in adaptive radiations. PLoS Biol. 4:e373.

Gibbs, R. A., G. M. Weinstock, M. L. Metzker, D. M. Muzny, E. J. Sodergren, S. Scherer, G. Scott, D. Steffen, K. C. Worley, P. E. Burch, et al. 2004. Genome sequence of the Brown Norway rat yields insights into mammalian evolution. Nature 428:493–521.

Gibbs, R. A., J. Rogers, M. G. Katze, R. Bumgarner, R. A. Gibbs, G. M. Weinstock, and the Rhesus Macaque Genome Sequencing Consortium. 2007. Evolutionary and biomedical insights from the rhesus macaque genome. Science 316:222–234.

Gregory, T. R. 2007. Animal genome size database. http://www.genomesize.com.

Guindon, S., and O. Gascuel. 2003. A simple, fast, and accurate algorithm to estimate large phylogenies by maximum likelihood. Syst. Biol. 52:696–704.

Haddrill, P. R., K. R. Thornton, B. Charlesworth, and P. Andolfatto. 2005. Multilocus patterns of nucleotide variability and the demographic and selection history of *Drosophila melanogaster* populations. Genome Res. 15:790–799.

Haddrill, P. R., D. L. Halligan, D. Tomaras, and B. Charlesworth. 2007. Reduced efficacy of selection in regions of the *Drosophila* genome that lack crossing over. Genome Biol. 8:R18.

Hall, M. C., and J. H. Willis. 2005. Transmission ratio distortion in intraspecific hybrids of *Mimulus guttatus*: implications for genomic divergence. Genetics 170:375–386.

Hansen, T. F. 1997. Stabilizing selection and the comparative analysis of adaptation. Evolution 51:1341–1351.

Hassold, T., and P. Hunt. 2001. To ERR (meiotically) is human: the genesis of human aneuploidy. Nat. Rev. Genet. 2:280–291.

Hayman, D. L., and P. G. Martin. 1974. Chordata 4. Gebruder Bortraeger, Berlin.

Hayman, D. L., H. D. M. Moore, and E. P. Evans. 1988. Further evidence of novel sex differences in chiasma distributions in marsupials. Heredity 61:455–458.

Hill, W. G., and A. Robertson. 1966. Effect of linkage on limits to artificial selection. Genet. Res. 8:269–294.

Huelsenbeck, J. P., and F. Ronquist. 2005. Bayesian analysis of molecular evolution using MrBayes. Pp. 182–232 *in* R. Nielsen, ed. Statistical Methods in Molecular Evolution. Springer, New York.

Hulten, M. 1974. Chiasma distribution at diakinesis in normal human male. Hereditas 76:55–78.

Ihara, N., A. Takasuga, K. Mizoshita, H. Takeda, M. Sugimoto, Y. Mizoguchi, T. Hirano, T. Itoh, T. Watanabe, K. M. Reed, et al. 2004. A comprehensive genetic map of the cattle genome based on 3802 microsatellites. Genome Res. 14:1987–1998.

Jeffreys, A. J., and R. Neumann. 2002. Reciprocal crossover asymmetry and meiotic drive in a human recombination hot spot. Nat. Genet. 31:267–271.

Jeffreys, A. J., J. Murray, and R. Neumann. 1998. High-resolution mapping of crossovers in human sperm defines a minisatellite-associated recombination hotspot. Mol. Cell 2:267–273.

Jensen-Seaman, M. I., T. S. Furey, B. A. Payseur, Y. T. Lu, K. M. Roskin, C. F. Chen, M. A. Thomas, D. Haussler, and H. J. Jacob. 2004. Comparative recombination rates in the rat, mouse, and human genomes. Genome Res. 14:528–538.

Jones, G. H. 1984. The control of chiasma distribution. Symposia of the Society for Experimental Biology 38:293–320.

Kidwell, M. G. 1972. Genetic change of recombination value in *Drosophila melanogaster*. I. Artificial selection for high and low recombination and some properties of recombination-modifying genes. Genetics 70:419–432.

Koehler, K. E., R. S. Hawley, S. Sherman, and T. Hassold. 1996. Recombination and nondisjunction in humans and flies. Hum. Mol. Genet. 5:1495–1504.

Kondrashov, A. S. 1988. Deleterious mutations and the evolution of sexual reproduction. Nature 336:435–440.

Kong, A., D. F. Gudbjartsson, J. Sainz, G. M. Jonsdottir, S. A. Gudjonsson, B. Richardsson, S. Sigurdardottir, J. Barnard, B. Hallbeck, G. Masson, T. Thorgeirsson, M. L. Frigge, et al. 2002. A high-resolution recombination map of the human genome. Nat. Genet. 31:241–247.

Kong, A., J. Barnard, D. F. Gudbjartsson, G. Thorleifsson, G. Jonsdottir, S. Sigurdardottir, B. Richardsson, J. Jonsdottir, T. Thorgeirsson, M. L. Frigge, et al. 2004. Recombination rate and reproductive success in humans. Nat. Genet. 36:1203–1206.

Kriegs, J. O., G. Churakov, M. Kiefmann, U. Jordan, J. Brosius, and J. Schmitz. 2006. Retroposed elements as archives for the evolutionary history of placental mammals. PLoS Biol. 4:537–544.

Lander, E. S., L. M. Linton, B. Birren, C. Nusbaum, M. C. Zody, J. Baldwin, K. Devon, K. Dewar, M. Doyle, W. Fitz-Hugh, et al. 2001. Initial sequencing and analysis of the human genome. Nature 409:860–921.

Lenormand, T. 2003. The evolution of sex dimorphism in recombination. Genetics 163:811–822.

Lenormand, T., and S. P. Otto. 2000. The evolution of recombination in a heterogeneous environment. Genetics 156:423–438.

Lin, Y. H., P. A. McLenachan, A. R. Gore, M. J. Phillips, R. Ota, M. D. Hendy, and D. Penny. 2002. Four new mitochondrial genomes and the increased stability of evolutionary trees of mammals from improved taxon sampling. Mol. Biol. Evol. 19:2060–2070.

Lindblad-Toh, K., C. M. Wade, T. S. Mikkelsen, E. K. Karlsson, D. B. Jaffe, M. Kamal, M. Clamp, J. L. Chang, E. J. Kulbokas, M. C. Zody, et al. 2005. Genome sequence, comparative analysis and haplotype structure of the domestic dog. Nature 438:803–819.

Lynch, M. 1991. Methods for the analysis of comparative data in evolutionary biology. Evolution 5:1065–1080.

Lynch, M., and W. G. Hill. 1986. Phenotypic evolution by neutral mutation. Evolution 40:915–935.

Maddox, J. F., K. P. Davies, A. M. Crawford, D. J. Hulme, D. Vaiman, E. P. Cribiu, B. A. Freking, K. J. Beh, N. E. Cockett, N. Kang, et al. 2001. An enhanced linkage map of the sheep genome comprising more than 1000 loci. Genome Res. 11:1275–1289.

Madsen, O., M. Scally, C. J. Douady, D. J. Kao, R. W. DeBry, R. Adkins, H. M. Amrine, M. J. Stanhope, W. W. de Jong, and M. S. Springer.. 2001. Parallel adaptive radiations in two major clades of placental mammals. Nature 409:610–614.

Marshall Graves, J. A., M. J. Wakefield, M. B. Renfree, D. W. Cooper, T. Speed, K. Lindblad-Toh, E. S. Lander, and R. K. Wilson. 2004. Proposal to sequence the genome of the model marsupial *Macropus eugenii* (Tammar wallaby). http://www.genome.gov/Pages/Research/Sequencing/SeqProposals/WallabySEQ.pdf

Mather, K. 1938. Crossing-over. Biol. Rev. 13:252–292.

Maynard Smith, J. 1971. What Use Is Sex? J. Theor. Biol. 30:319–335.

Maynard Smith, J., and J. Haigh. 1974. Hitch-hiking effect of a favorable gene. Genet. Res. 23:23–35.

Menotti-Raymond, M., V. A. David, L. A. Lyons, A. A. Schaffer, J. F. Tomlin, M. K. Hutton, and S. J. O'Brien. 1999. A genetic linkage map of microsatellites in the domestic cat (*Felis catus*). Genomics 57:9–23.

Michod, R. E., and B. R. Levin. 1988. The evolution of sex. Sinauer Press, Sunderland, MA.

Micic, M., S. Micic, and V. Diklic. 1982. Low chiasma frequency as an etiological factor in male infertility. Clin. Genet. 22:266–269.

Mikkelsen, T. S., M. J. Wakefield, B. Aken, C. T. Amemiya, J. L. Chang, S. Duke, M. Garber, A. J. Gentles, L. Goodstadt, A. Heger, et al. 2007. Genome of the marsupial *Monodelphis domestica* reveals innovation in non-coding sequences. Nature 447:167–178.

Mukherjee, A. S. 1961. Effect of selection on crossing over in the males of *Drosophila anassae*. Am. Nat. 95:57–59.

Muller, H. J. 1932. Some genetic aspects of sex. Am. Nat 66:118–138.

——. 1964. The relation of recombination to mutational advance. Mutat. Res. 106:2–9.

Murphy, W. J., E. Eizirik, S. J. O'Brien, O. Madsen, M. Scally, C. J. Douady, E. Teeling, O. A. Ryder, M. J. Stanhope, W. W. de Jong, et al. 2001. Resolution of the early placental mammal radiation using Bayesian phylogenetics. Science 294:2348–2351.

Murphy, W. J., E. Eizirik, S. J. O'Brien, O. Madsen, M. Scally, et al. 2001b. Resolution of the early placental mammal radiation using Bayesian phylogenetics. Science 294:2348–2351.

Myers, S., L. Bottolo, C. Freeman, G. McVean, and P. Donnelly. 2005. A fine-scale map of recombination rates and hotspots across the human genome. Science 310:321–324.

Neff, M. W., K. W. Broman, C. S. Mellersh, K. Ray, G. M. Acland, G. D. Aguirre, J. S. Ziegle, E. A. Ostrander, and J. Rine. 1999. A second-generation genetic linkage map of the domestic dog, *Canis familiaris*. Genetics 151:803–820.

Neff, M. W., A. Wong, A. Ruhe, S. Bruce, K. Robertson, J. Ziegle, and K. W. Broman. 2006. A comprehensive linkage map of the dog genome. Third International Conference. Advances in Canine and Feline Genomics, August 2–5. http://www.vgl.ucdavis.edu/research/canine/projects/linkage_map/.

Neumann, R., and A. J. Jeffreys. 2006. Polymorphism in the activity of human crossover hotspots independent of local DNA sequence variation. Hum. Mol. Genet. 15:1401–1411.

Nowak, R. M. 1999a. Walker's Mammals of the World, Volume I, 6th Edition. The Johns Hopkins Univ. Press, Baltimore, MD.

——. 1999b. Walker's Mammals of the World, Volume II, 6th Edition. The Johns Hopkins Univ. Press, Baltimore, MD.

O'Meara, B. C., C. Ane, M. J. Sanderson, and P. C. Wainwright. 2006. Testing for different rates of continuous trait evolution using likelihood. Evolution 60:922–933.

Paradis, E., J. Claude, and K. Strimmer. 2004. APE: analyses of phylogenetics and evolution in R language. Bioinformatics 20:289–290.

Pardo-Manuel de Villena, F., and C. Sapienza. 2001. Recombination is proportional to the number of chromosome arms in mammals. Mamm. Genome 12:318–322.

Parsons, P. A. 1958. Selection for increased recombination in *Drosophila melanogaster*. Am. Nat. 92:255–256.

Peters, A. D., and C. M. Lively. 1999. The red queen and fluctuating epistasis: a population genetic analysis of antagonistic coevolution. Am. Nat. 154:393–405.

Ptak, S. E., A. D. Roeder, M. Stephens, Y. Gilad, S. Paabo, and M. Przeworski. 2004. Absence of the TAP2 human recombination hotspot in chimpanzees. PLoS Biol. 2:849–855.

Ptak, S. E., D. A. Hinds, K. Koehler, B. Nickel, N. Patil, D. G. Ballinger, M. Przeworski, K. A. Frazer, and S. Paabo. 2005. Fine-scale recombination patterns differ between chimpanzees and humans. Nat. Genet. 37:429–434.

R Development Core Team. 2006. R: a language and environment for statistical computing. R Foundation for Statistical Computing, Vienna, Austria.

Rogers, J., M. C. Mahaney, S. M. Witte, S. Nair, D. Newman, S. Wedel, L. A. Rodriguez, K. S. Rice, S. H. Slifer, A. Perelygin, et al. 2000. A genetic linkage map of the baboon (*Papio hamadryas*) genome based on human microsatellite polymorphisms. Genomics 67:237–247.

Rogers, J., R. Garcia, W. Shelledy, J. Kaplan, A. Arya, Z. Johnson, M. Bergstrom, L. Novakowski, P. Nair, A. Vinson, et al. 2006. An initial genetic linkage map of the rhesus macaque (*Macaca mulatta*) genome using human microsatellite loci. Genomics 87:30–38.

Rohrer, G. A., L. J. Alexander, Z. L. Hu, T. P. L. Smith, J. W. Keele, and C. W. Beattie. 1996. A comprehensive map of the porcine genome. Genome Res. 6:371–391.

Rohrer, G., J. E. Beever, M. F. Rothschild, L. Schook, R. Gibbs, and G. Weinstock. 2002. Porcine Genome Sequencing Initiative. http://www.genome.gov/Pages/Research/Sequencing/SeqProposals/PorcineSEQ021203.pdf

Ronquist, F., and J. P. Huelsenbeck. 2003. MrBayes 3: Bayesian phylogenetic inference under mixed models. Bioinformatics 19:1572–1574.

Ross-Ibarra, J. 2004. The evolution of recombination under domestication: a test of two hypotheses. Am. Nat. 163:105–112.

Samollow, P. B., C. M. Kammerer, S. M. Mahaney, J. L. Schneider, S. J. Westenberger, J. L. VandeBerg, and E. S. Robinson. 2004. First-generation linkage map of the gray, short-tailed opossum, *Monodelphis domestica*, reveals genome-wide reduction in female recombination rates. Genetics 166:307–329.

Shah, K., G. Sivapalan, N. Gibbons, H. Tempest, and D. K. Griffin. 2003. The genetic basis of infertility. Reproduction 126:13–25.

Sharp, P. J., and D. L. Hayman. 1988. An examination of the role of chiasma frequency in the genetic system of marsupials. Heredity 60:77–85.

Shifman, S., J. Tzenova Bell, R. R. Copley, M. S. Taylor, R. W. Williams, R. Mott, and J. Flint. 2006. A high-resolution single nucleotide polymorphism genetic map of the mouse genome. PLoS Biol. 4:e395.

Shiroishi, T., T. Koide, M. Yoshino, T. Sagai, and K. Moriwaki. 1995. Hotspots of homologous recombination in mouse meiosis. Adv. Biophys. 31:119–132.

Smith, F. A., J. H. Brown, J. P. Haskell, S. K. Lyons, J. Alroy, E. L. Charnov, T. Dayan, B. J. Enquist, S. K. M. Ernest, E. A. Hadly, et al. 2004. Similarity of mammalian body size across the taxonomic hierarchy and across space and time. Am. Nat. 163:672–691.

Springer, M. S., M. J. Stanhope, O. Madsen, and W. W. de Jong. 2004. Molecules consolidate the placental mammal tree. Trends Ecol. Evol. 19:430–438.

Steen, R. G., A. E. Kwitek-Black, C. Glenn, J. Gullings-Handley, W. Van Etten, O. S. Atkinson, D. Appel, S. Twigger, M. Muir, T. Mull, et al. 1999. A high-density integrated genetic linkage and radiation hybrid map of the laboratory rat. Genome Res. 9:Ap1–Ap8.

Swinburne, J. E., M. Boursnell, G. Hill, L. Pettitt, T. Allen, B. Chowdhary, T. Hasegawa, M. Kurosawa, T. Leeb, S. Mashima, et al. 2006. Single linkage group per chromosome genetic linkage map for the horse, based on two three-generation, full-sibling, crossbred horse reference families. Genomics 87:1–29.

The International HapMap Consortium. 2005. A haplotype map of the human genome. Nature 437:1299–1320.

Thompson, J. D., D. G. Higgins, and T. J. Gibson. 1994. Clustal-W: improving the sensitivity of progressive multiple sequence alignment through sequence weighting, position-specific gap penalties and weight matrix choice. Nucleic Acids Res. 22:4673–4680.

True, J. R., J. M. Mercer, and C. C. Laurie. 1996. Differences in crossover frequency and distribution among three sibling species of Drosophila. Genetics 142:507–523.

Venter, J. C., M. D. Adams, E. W. Myers, P. W. Li, R. J. Mural, G. G. Sutton, H. O. Smith, M. Yandell, C. A. Evans, R. A. Holt, et al. 2001. The sequence of the human genome. Science 291:1304–1351.

Voight, B. F., S. Kudaravalli, X. Q. Wen, and J. K. Pritchard. 2006. A map of recent positive selection in the human genome. PLoS Biol. 4:446–458.

Waddell, P. J., H. Kishino, and R. Ota. 2001. A phylogenetic foundation for comparative mammalian genomics. Genome Informatics 12:141–154.

Waterston, R. H., K. Lindblad-Toh, E. Birney, J. Rogers, J. F. Abril, P. Agarwal, R. Agarwala, R. Ainscough, M. Alexandersson, P. An, et al. 2002. Initial sequencing and comparative analysis of the mouse genome. Nature 420:520–562.

Winckler, W., S. R. Myers, D. J. Richter, R. C. Onofrio, G. J. McDonald, R. E. Bontrop, G. A. T. McVean, S. B. Gabriel, D. Reich, P. Donnelly

et al. 2005. Comparison of fine-scale recombination rates in humans and chimpanzees. Science 308:107–111.

Wu, T. C., and M. Lichten. 1995. Factors that affect the location and frequency of meiosis-induced double-strand breaks in *Saccharomyces cerevisiae*. Genetics 140:55–66.

Xu, X. F., A. Janke, and U. Arnason. 1996. The complete mitochondrial DNA sequence of the greater Indian rhinoceros, Rhinoceros unicornis, and the phylogenetic relationship among Carnivora, Perissodactyla, and Artiodactyla (plus Cetacea). Mol. Biol. Evol. 13:1167–1173.

Yauk, C. L., P. R. J. Bois, and A. J. Jeffreys. 2003. High-resolution sperm typing of meiotic recombination in the mouse MHC E-beta gene. EMBO J. 22:1389–1397.

Zenger, K. R., L. M. McKenzie, and D. W. Cooper. 2002. The first comprehensive genetic linkage map of a marsupial: the tammar wallaby (*Macropus eugenii*). Genetics 162:321–330.

Zetka, M. C., and A. M. Rose. 1995. Mutant *Rec-1* eliminates the meiotic pattern of crossing-over in *Caenorhabditis elegans*. Genetics 141:1339–1349.

Associate Editor: J. True

Supplementary Material

The following supplementary material is available for this article:

Figure S1. Majority rule consensus (50%) Bayesian phylogenetic tree for the (**A**) CFTR and (**B**) the mitochondrial sequence alignments.

Table S1. CFTR coding sequence accession numbers.

Table S2. Alternative models of molecular evolution applied to a CFTR coding sequence alignment of 13 mammalian species and the outgroup taxon platypus.

Table S3. Alternative models of molecular evolution applied to a concatenated mitochondrial protein coding sequence alignment of 13 mammalian species and the outgroup taxon platypus.

This material is available as part of the online article from:
http://www.blackwell-synergy.com/doi/abs/10.1111/j.1558-5646.2007.00278.x
(This link will take you to the article abstract).

Please note: Blackwell Publishing is not responsible for the content or functionality of any supplementary materials supplied by the authors. Any queries (other than missing material) should be directed to the corresponding author for the article.